



A northward shift of the North Atlantic Ocean Intertropical Convergence Zone in response to summertime Saharan dust outbreaks

Eric M. Wilcox,¹ K. M. Lau,¹ and Kyu-Myong Kim¹

Received 22 November 2009; revised 13 January 2010; accepted 25 January 2010; published 23 February 2010.

[1] The influence on the summertime North Atlantic Ocean inter-tropical convergence zone (ITCZ) of Saharan dust outbreaks is explored using nine years of continuous satellite observations and atmospheric reanalysis products. During dust outbreak events rainfall along the ITCZ shifts northward by 1 to 4 degrees latitude. Dust outbreaks coincide with warmer lower-tropospheric temperatures compared to low dust conditions, which is attributable to advection of the warm Saharan Air Layer, enhanced subtropical subsidence, and radiative heating of dust. The enhanced positive meridional temperature gradient coincident with dust outbreaks is accompanied by an acceleration of the easterly winds on the north side of the African Easterly Jet (AEJ). The center of the positive vorticity region south of the AEJ moves north drawing the center of low-level convergence and ITCZ rainfall northward with it. The enhanced precipitation on the north side of the ITCZ occurs in spite of widespread sea surface temperature cooling north of the ITCZ owing to reduced surface solar insolation by dust scattering. **Citation:** Wilcox, E. M., K. M. Lau, and K.-M. Kim (2010), A northward shift of the North Atlantic Ocean Intertropical Convergence Zone in response to summertime Saharan dust outbreaks, *Geophys. Res. Lett.*, 37, L04804, doi:10.1029/2009GL041774.

1. Introduction

[2] Saharan dust outbreaks transport large plumes of dust across the northern tropical and subtropical Atlantic Ocean [Carlson and Prospero, 1972]. Accompanying the dust is the warm dry air mass known as the Saharan Air Layer (SAL), which resides in a thick layer above the marine boundary layer [Karyampudi and Carlson, 1988]. The positive meridional temperature gradient associated with the SAL gives rise to the African Easterly Jet (AEJ), a dynamically unstable westward jet in the zonal wind field centered on roughly 15° N latitude and the 650 hPa pressure level during summer [Burpee, 1972; Cook, 1999]. Wave disturbances along the southern edge AEJ provide a major source of variability in summer precipitation along the Inter-tropical convergence zone (ITCZ) centered on roughly 5° N latitude [Burpee, 1972; Reed et al., 1977; Diedhiou et al., 1999]. Although principal zonal axes of the ITCZ and the SAL are

separated by about 10° of latitude, the modulation of the AEJ in response to variations in the meridional temperature gradient associated with the SAL and its periodic dust outbreaks provides a mechanism for the SAL to modulate precipitation along the ITCZ. This study applies nine years of summertime observations from the Earth Observing System network of satellites to explore the response of precipitation along the Atlantic ITCZ to dust outbreaks over the Northern Atlantic Ocean.

[3] The dust aerosol optical depth (AOD) over the North Atlantic Ocean is observed to peak during the summer, and the main latitude of dust transport migrates seasonally by about 10° to 20° together with the seasonal migration of the ITCZ [Kaufman et al., 2005]. Dust mobilized by strong winds at the surface is mixed vertically by dry convection, resulting in a well-mixed layer of dry dusty air extending from the surface to as high as the 500 hPa pressure level over the desert. As this dust-laden Saharan Air Layer (SAL) moves westward over the North Atlantic Ocean it is undercut by the cooler marine boundary layer air. This leaves the SAL as a well-intact and nearly homogeneously mixed layer from approximately 850 hPa to 500 hPa with a nearly uniform potential temperature [Carlson and Prospero, 1972]. Dust and the SAL propagate across the ocean, with the top of the SAL lowering approximately 50 hPa and the SAL base rising [Karyampudi and Carlson, 1988; Karyampudi et al., 1999]. The dry SAL with uniform elevated potential temperature established over the continent is maintained as the SAL is transported as far as 40°W over the North Atlantic Ocean. East of this longitude, the shortwave heating of dust is sufficient to balance the longwave cooling of the column. Further west, longwave cooling erodes the SAL except in cases where the AOD exceeds 0.6 [Wong et al., 2009].

[4] An idealized experiment with an atmospheric general circulation model indicates that dust radiative heating results in a systematic increase and northward latitudinal displacement of ITCZ precipitation [Randall et al., 1984]. A more recent simulation study [Lau et al., 2009] finds evidence for a strengthening of the West African monsoon owing to the radiative effect of the dust that is manifest in a northward shift of precipitation in the Eastern Atlantic and Western Africa land region. Using satellite data, Huang et al. [2009] find that precipitation on the southern edge of the Atlantic ITCZ is reduced in months with high dust loading compared with months with low dust loading throughout much of the year, however precipitation is enhanced north of the Atlantic ITCZ during summer months. This study seeks to characterize the detectable response of summertime oceanic ITCZ precipitation in the satellite record that is dynamically

¹Laboratory for Atmospheres, NASA Goddard Space Flight Center, Greenbelt, Maryland, USA.

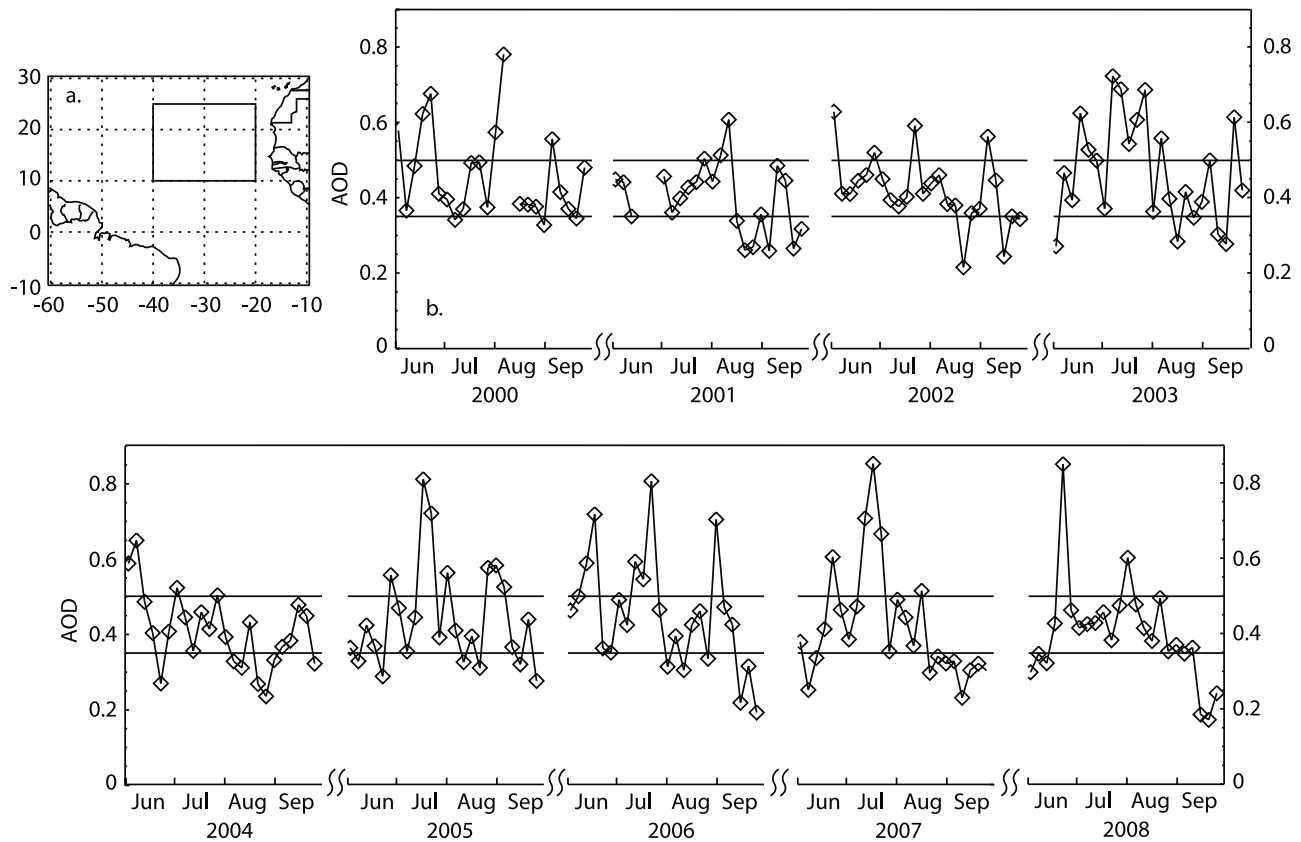


Figure 1. (a) The box 20° to 40° W and 10° to 25° N indicates the region over which pentad-mean MODIS AOD from the Terra satellite is averaged to identify pentads coinciding with dust outbreak events. (b) Nine-year JJAS time-series of pentad-mean AOD averaged over the box shown in Figure 1a. Horizontal lines at AOD = 0.5 and 0.35 indicate the upper and lower quartiles.

connected to the warm tropospheric temperatures coinciding with dust outbreak events.

2. Data and Methodology

[5] Observations of the optical depth of aerosols (AOD), precipitation (P), 600hPa zonal winds (u600), atmospheric temperature (T), and sea surface temperature (SST) are taken from nine years of satellite data and reanalysis products spanning nearly the entire lifetime of the NASA Terra satellite (2000–2008). AOD at 0.55 μm is obtained at 1° resolution from the level 3 collection 5 atmosphere products of the MODIS instrument on Terra [Remer *et al.*, 2008]. Three-hourly precipitation data is obtained at 0.25° resolution from the NASA Tropical Rainfall Measuring Mission (TRMM) 3B42 dataset, a merged product of several satellite rain rate estimates [Huffman *et al.*, 2007]. T and u600 are taken from the NCEP/NCAR reanalysis [Kalnay *et al.*, 1996]. Monthly-mean SST is obtained at 1° resolution from the TRMM Microwave Imager [Wentz *et al.*, 2000]. All five quantities are obtained for the June through September period (JJAS) 2000–2008. Quarter-degree values of P are averaged over the 1° grid common to the other data sets. Once daily AOD, six-times daily P, and four-times daily T and u600 are further averaged over pentads in order to capture the major dust outbreak events spanning several days and smooth over daily variability.

[6] The time series of pentad-mean AOD averaged over the region 20°–40° W lon., 10°–25° N lat. (referred to below as the AOD reference box) during the JJAS season is shown in Figure 1. Pentads associated with dust outbreaks are identified by area- and pentad-averaged AOD greater 0.5, which coincides with the 75th percentile value of all area- and pentad-averaged AOD values. The episodic nature of dust outbreak events during the summer season is clearly indicated. Many events are brief and are limited to a single pentad. However, it is not uncommon for elevated dust levels to persist over two or three pentads. Significant inter-annual variability in the number and magnitude of major dust events is also evident. The impacts of dust outbreaks on temperature, winds and precipitation of the North Atlantic Ocean is evaluated from differences between pentad-mean conditions when AOD in the reference box exceeds the upper quartile (AOD > 0.5) and pentad-mean conditions corresponding AOD values in the reference box less than the lower quartile (AOD < 0.35). All differences shown exceed the 95% confidence level estimated as 1.96 times the standard deviation of the mean observed variability except where indicated. We limit our analysis to the response of the atmosphere over the ocean to dust outbreak events because of limitations in retrieving AOD over the bright desert surface. MODIS provides a stable continuous nine-year record of AOD over the ocean derived from radiance measurements regularly calibrated on-board the satellite. A

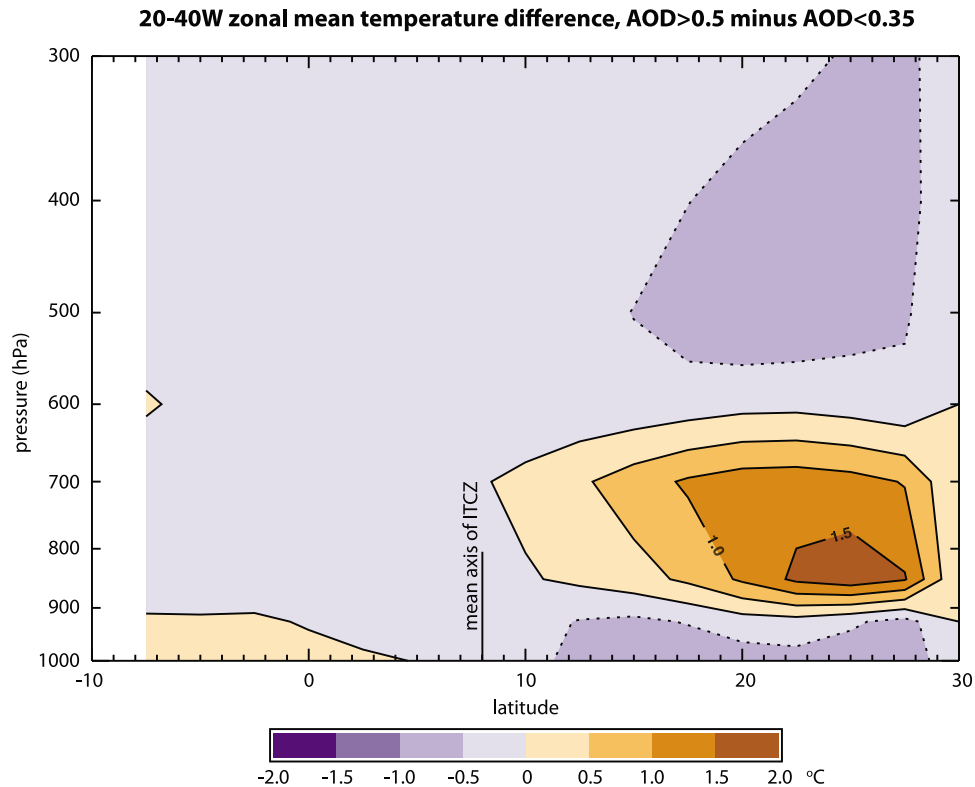


Figure 2. Difference between dust outbreak and low dust conditions of the zonal-mean T profile averaged 20° to 40° W (in °C).

similar stably calibrated record over the desert of comparable duration is not available at present.

3. Results

[7] Significant warming of the lower troposphere accompanies the transport of dust during outbreak events. Figure 2 shows the vertical and meridional distribution of T differences averaged 20°–40° W lon., west of the African continent, between dust outbreak and low AOD conditions in the reference box area (Figure 1). The warm temperatures associated with dust outbreaks occur within the SAL between 900 and 600 hPa and extend broadly from 10° to 30° N. On average during the JJAS season there exists a lower-tropospheric positive meridional temperature gradient, which is enhanced during dust outbreaks. All T differences greater than 0 in Figure 2 are statistically significant at greater than the 95% confidence level. Warming is attributable to westward advection of the warm Saharan Air Layer [Carlson and Prospero, 1972], subsidence of mid-tropospheric air [Karyampudi et al., 1999; Petit et al., 2005], and dust radiative heating [Carlson and Benjamin, 1980; Alpert et al., 1998; Zhu et al., 2007; Wong et al., 2009]. Additionally, the cooling near the surface below the SAL may be due to the shielding of solar radiation by dust [Lau et al., 2009]. The maximum of the warm temperature signature of dust outbreaks is centered between 20° and 30° N, well north of the central axis of dust transport centered on about 15°–18° N [Kaufman et al., 2005], indicating the importance of dynamical processes in the SAL for producing the thermal signature coincident with dust out-

breaks. Heating attributable to absorption of solar energy by dust may also be contributing to the elevated tropospheric temperatures. Estimated heating rates for typical dust outbreak events range from 0.2 K d⁻¹ [Alpert et al., 1998] to as much as 1 K d⁻¹ [Carlson and Benjamin, 1980], with more recent results suggesting a range from 0.2 to 0.4 K d⁻¹ [Zhu et al., 2007; Wong et al., 2009]. The southern boundary of the statistically significant region of elevated temperature occurs at 10° to 12° N lat. Convection is enhanced here, as discussed further below, suggesting that latent heating from the enhanced convection is contributing to the elevated temperatures at these latitudes.

[8] The African Easterly Jet lies above the positive meridional gradient in the seasonal-mean lower tropospheric temperature pattern as dictated by the thermal wind relation [e.g. Burpee, 1972]. This gradient, and the wind speed in the AEJ, peak at 15° N. The high T values associated with dust outbreaks peak to the north of the AEJ (Figure 2) enhancing the background positive meridional temperature gradient. The strongest enhancement of the meridional temperature gradient occurs at about 20° N along the northern boundary of the AEJ. The 600 hPa wind difference between dust outbreaks and low dust conditions is shown in Figure 3. The AEJ is accelerated during dust outbreak events by approximately 4 m s⁻¹ compared to low dust conditions at 20° N (averaged 20° to 40° W). This is an acceleration of about 50% of the mean AEJ velocity along its climatological axis, and the maximum acceleration occurs 4° to 5° north of the mean AEJ axis. Because dust outbreak events coincide with tropospheric warming well north of the AEJ axis, they also coincide with a strong acceleration of the northern side of

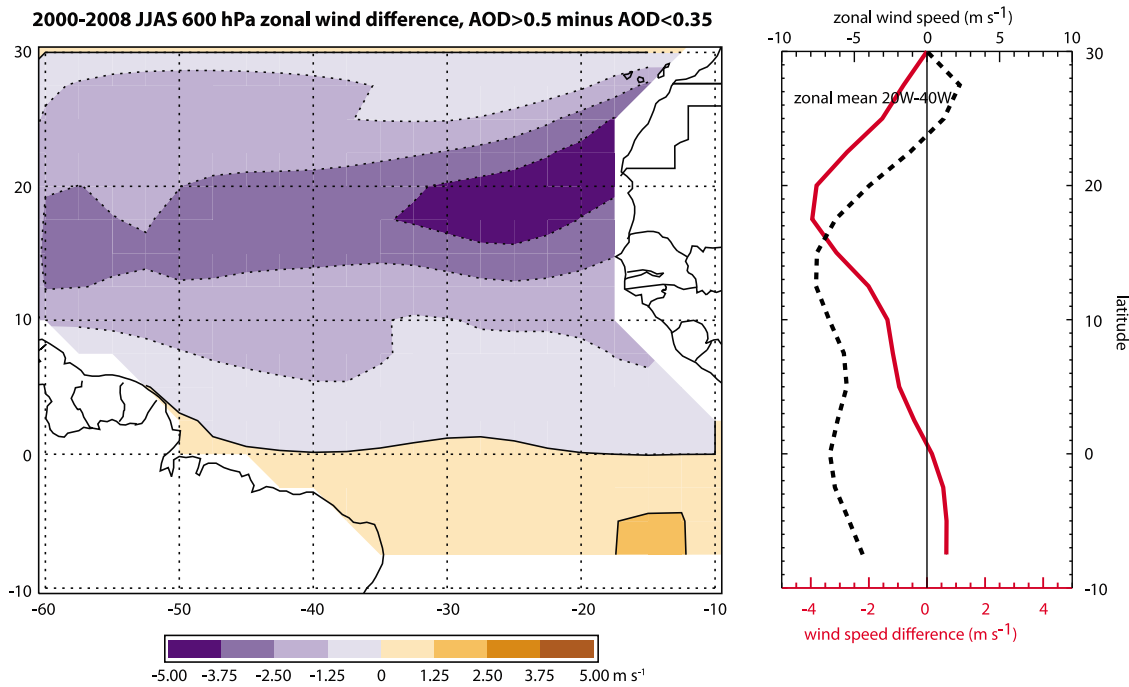


Figure 3. Difference between dust outbreak conditions and low AOD conditions for u_{600} . (left) Spatial distribution of the difference. (right) Zonal-mean averaged 20° to 40° W by latitude of the u_{600} difference (red, lower scale) and u_{600} averaged over low AOD pentads (dashed, upper scale).

2000-2008 JJAS precipitation difference, AOD > 0.5 minus AOD < 0.35

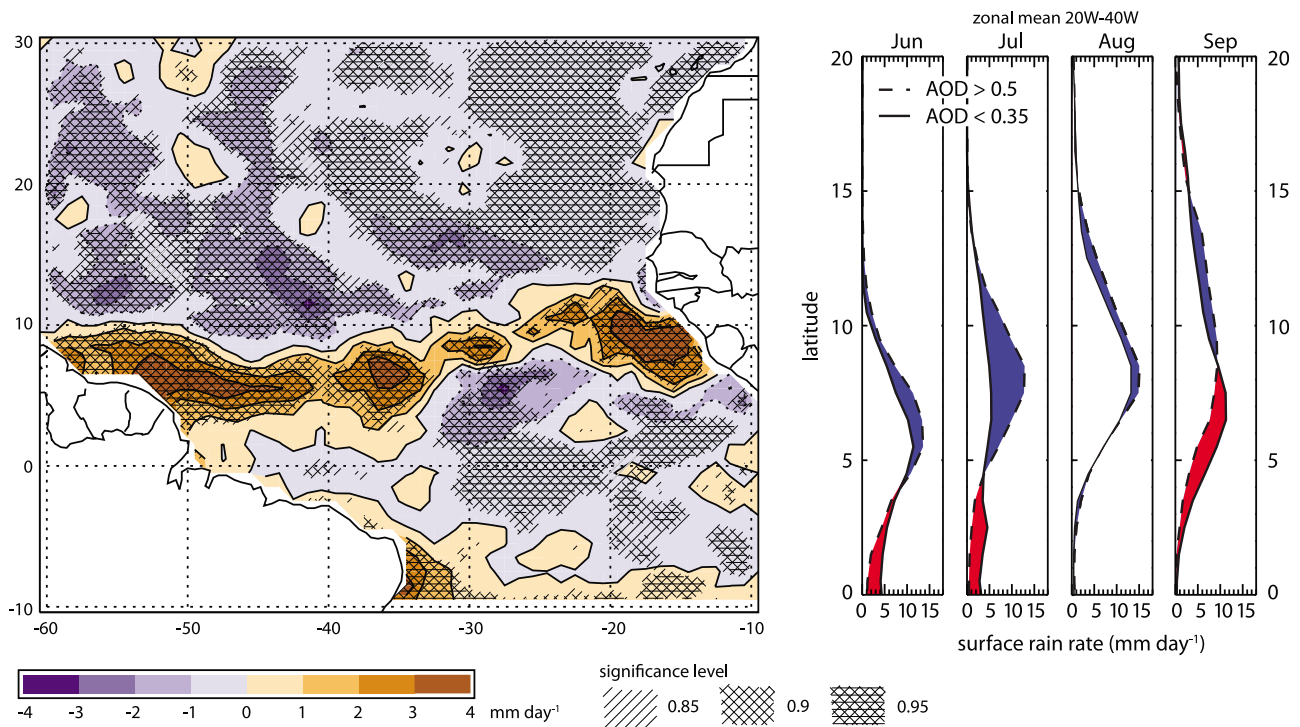


Figure 4. Difference in P (in mm d^{-1}) between dust outbreak conditions and low dust conditions. (left) Spatial distribution where the degree of hatching indicates level of significance of the difference compared to variability of pentad averages. The mean position of the ITCZ during the JJAS season is 8°N latitude. (right) Zonal-mean averaged 20° to 40° W by latitude of P during dust outbreak conditions (dashed) and low dust conditions (solid). Higher values during dust outbreaks denoted in blue, and lower values in red.

the AEJ, and a weaker acceleration of the core and southern side of the AEJ. The orientation of the jet acceleration in relation to the mean velocity of the jet, also shown in Figure 3, indicates that the meridional wind shear on either flank of the AEJ is increased. All u_{600} values less than zero (easterly differences) are significant to greater than 95%.

[9] The precipitation difference between dust outbreak conditions and low dust conditions is shown in Figure 4. During dust outbreaks there is a general increase in precipitation along the ITCZ compared to low dust conditions, and reductions in precipitation at several locations to the north and south of the ITCZ. In the region 20° to 40° W, directly south of the AOD reference box and offshore of the continent, precipitation is enhanced along the north side of the ITCZ and reduced on the south side of the ITCZ. There is a significant meridional migration of the ITCZ during the JJAS season. Also shown in Figure 4 is the nine-year average for each month of zonal mean P by latitude averaged 20° to 40° W for dust outbreak and low dust conditions. Increases in P during dust outbreak conditions are indicated in blue and reduction in red. There is a northward shift of the ITCZ in dust outbreak conditions compared to low dust conditions in each month ranging from 1° to 4° latitude. For the average of the JJAS season, the maximum increase in precipitation is centered on 11° N latitude, which is approximately the same latitude as the maximum increase in the 600 hPa easterly shear anomaly on the southern edge of the AEJ (Figure 3), and therefore coincides with the maximum increase in positive vorticity. The concurrent northward shift of the AEJ and the ITCZ convection reflect the observed association of precipitation in the vicinity of West Africa with the strength and location of the AEJ [Rowell *et al.*, 1992].

[10] The dynamics of the ITCZ is tightly coupled to variability of the SST pattern. For example, the meridional migration of the ITCZ with the seasons coincides with a meridional migration of the SST pattern [Waliser and Gautier, 1993]. This results from the correlation of strong convection with warm SSTs [e.g., Graham and Barnett, 1987]. In spite of that, the difference from low dust conditions of SST during dust outbreak conditions is -1.0° C north of the ITCZ and $+0.5^{\circ}$ C south of the ITCZ. The cooler temperatures beneath the dust outflow region north of the ITCZ is attributable to the radiative cooling of the surface owing to scattering by aerosols, as demonstrated by Lau and Kim [2007]. A northward shift of the ITCZ might be expected with higher SSTs north of the ITCZ, however this is opposite to the difference in the SST pattern during dust outbreak conditions. The observed northward shift in ITCZ precipitation during dust outbreaks is opposite to the response expected from cooler SSTs north of the ITCZ and warmer SSTs south of the ITCZ.

4. Summary

[11] Outbreaks of Saharan dust over the Atlantic Ocean during summer are found to coincide with a northward shift of ITCZ precipitation of 1 to 4 degrees latitude. This response, which runs counter to the cooling of SSTs north of the ITCZ during outbreaks, helps explain why the mean position of the ITCZ closely coincides with the southern edge of the SAL. A mechanism for the ITCZ shift is suggested that links the lower-tropospheric warm temperature signature of dust outbreaks on the northern edge of the SAL

to the circulation between the ITCZ and the SAL. The warming of the SAL during outbreaks enhances the meridional temperature gradient at 850 hPa on the northern edge of the AEJ, thereby accelerating the jet preferentially north of the mean axis of the jet. The anomalous zonal wind pattern enhances the easterly shear and positive vorticity on the southern edge of the AEJ at 10° to 12° N, coinciding with the enhanced precipitation north of the mean ITCZ.

[12] Warming in the SAL during dust outbreaks is attributable to warm advection, subsidence, and radiative heating by dust. The peak of the outbreak warming is located well north of the mean axis of the dust outflow, indicating that dynamical processes in the SAL are important in producing the lower-tropospheric warming coincident with dust outbreaks. Estimates of net radiative heating in the dust layer during dust outbreaks range from 0.2 to 0.4 K d^{-1} [Alpert *et al.*, 1998; Zhu *et al.*, 2007; Wong *et al.*, 2009]. The pattern of enhanced precipitation several degrees north of the climatological ITCZ observed during dust outbreaks is similar to the adjustment found in atmospheric simulations in response to the addition of the dust radiative forcing [Randall *et al.*, 1984; Lau *et al.*, 2009]. This response is also consistent with the “elevated heat pump” mechanism of atmospheric heating, induced by solar forcing by absorbing aerosols for the Asian monsoon [Lau *et al.*, 2006] and the Atlantic ITCZ [Lau *et al.*, 2009].

[13] **Acknowledgments.** This work was supported by the NASA African Monsoon Multidisciplinary Activities program. NASA MODIS and TRMM data are archived at the NASA/GSFC. TMI SST data are produced by Remote Sensing Systems (www.remss.com). NCEP/NCAR Reanalysis products were obtained from NOAA/OAR/ESRL.

References

- Alpert, P., et al. (1998), Quantification of dust-forced heating of the lower troposphere, *Nature*, 395, 367–370, doi:10.1038/26456.
- Burpee, R. W. (1972), The origin and structure of easterly waves in the lower troposphere of North Africa, *J. Atmos. Sci.*, 29, 77–89, doi:10.1175/1520-0469(1972)029<0077:TOASOE>2.0.CO;2.
- Carlson, T. N., and S. G. Benjamin (1980), Radiative heating rates for Saharan dust, *J. Atmos. Sci.*, 37, 193–213, doi:10.1175/1520-0469(1980)037<0193:RHRFSD>2.0.CO;2.
- Carlson, T. N., and J. M. Prospero (1972), The large-scale movement of Saharan air outbreaks over the northern equatorial Atlantic, *J. Appl. Meteorol.*, 11, 283–297, doi:10.1175/1520-0450(1972)011<0283:TLMSOS>2.0.CO;2.
- Cook, K. H. (1999), Generation of the African Easterly Jet and its role in determining West African precipitation, *J. Clim.*, 12, 1165–1184, doi:10.1175/1520-0442(1999)012<1165:GOTAEJ>2.0.CO;2.
- Diedhiou, A., S. Janicot, A. Viltard, P. de Felice, and H. Laurent (1999), Easterly wave regimes and associated convection over West Africa and tropical Atlantic: Results from the NCEP/NCAR and ECMWF reanalysis, *Clim. Dyn.*, 15, 795–822, doi:10.1007/s003820050316.
- Graham, N. E., and T. P. Barnett (1987), Sea surface temperature, surface wind divergence, and convection over tropical oceans, *Science*, 238, 657–659, doi:10.1126/science.238.4827.657.
- Huang, J., C. Zhang, and J. M. Prospero (2009), Aerosol-induced large-scale variability in precipitation over the tropical Atlantic, *J. Clim.*, 22, 4970–4988, doi:10.1175/2009JCLI2531.1.
- Huffman, G. J., R. F. Adler, D. T. Bolvin, G. Gu, E. J. Nelkin, K. P. Bowman, Y. Hong, E. F. Stocker, and D. B. Wolff (2007), The TRMM multi-satellite precipitation analysis: Quasi-global, multi-year, combined-sensor precipitation estimates at fine scale, *J. Hydrometeorol.*, 8, 38–55, doi:10.1175/JHM560.1.
- Kalnay, E., et al. (1996), The NCEP/NCAR 40-year reanalysis project, *Bull. Am. Meteorol. Soc.*, 77, 437–470, doi:10.1175/1520-0477(1996)077<0437:TNYRP>2.0.CO;2.
- Karyampudi, V. M., and T. N. Carlson (1988), Analysis and numerical simulations of the Saharan air layer and its effect on easterly wave disturbances, *J. Atmos. Sci.*, 45, 3102–3136, doi:10.1175/1520-0469(1988)045<3102:AANSOT>2.0.CO;2.

- Karyampudi, V. M., et al. (1999), Validation of the Saharan dust plume conceptual model using lidar, Meteosat, and ECMWF data, *Bull. Am. Meteorol. Soc.*, *80*, 1045–1075, doi:10.1175/1520-0477(1999)080<1045:VOTSDP>2.0.CO;2.
- Kaufman, Y. J., I. Koren, L. A. Remer, D. Tanre, P. Ginoux, and S. Fan (2005), Dust transport and deposition observed from the Terra-Moderate Resolution Imaging Spectroradiometer (MODIS) spacecraft over the Atlantic Ocean, *J. Geophys. Res.*, *110*, D10S12, doi:10.1029/2003JD004436.
- Lau, K. M., and K. M. Kim (2007), Cooling of the Atlantic by Saharan dust, *Geophys. Res. Lett.*, *34*, L23811, doi:10.1029/2007GL031538.
- Lau, K. M., M. K. Kim, and K. M. Lau (2006), Aerosol induced anomalies in the Asian summer monsoon: The role of the Tibetan Plateau, *Clim. Dyn.*, *26*, 855–864, doi:10.1007/s00382-006-0114-z.
- Lau, K. M., K.-M. Kim, Y. C. Sud, and G. K. Walker (2009), A GCM study of the response of the atmospheric water cycle of West Africa and the Atlantic to Saharan dust radiative forcing, *Ann. Geophys.*, *27*, 4023–4037.
- Petit, R. H., M. Legrand, I. Jankowiak, J. Molinić, C. Asselin de Beauville, G. Marion, and J. L. Mansot (2005), Transport of Saharan dust over the Caribbean Islands: Study of an event, *J. Geophys. Res.*, *110*, D18S09, doi:10.1029/2004JD004748.
- Prospero, J. M., and T. N. Carlson (1980), Saharan air outbreaks over the tropical North Atlantic, *Pure Appl. Geophys.*, *119*, 677–691, doi:10.1007/BF00878167.
- Randall, D., T. Carlson, and Y. Mintz (1984), The sensitivity of a general circulation model to Saharan dust heating, in *Aerosols and Their Climatic Effects*, edited by H. E. Gerber and A. Deepak, pp. 123–132, A Deepak, Hampton, Va.
- Reed, R. J., D. C. Norquist, and E. E. Recker (1977), The structure and properties of African wave disturbances as observed during phase III of GATE, *Mon. Weather Rev.*, *105*, 317–333, doi:10.1175/1520-0493(1977)105<0317:TSAPOA>2.0.CO;2.
- Remer, L. A., et al. (2008), Global aerosol climatology from the MODIS satellite sensors, *J. Geophys. Res.*, *113*, D14S07, doi:10.1029/2007JD009661.
- Rowell, D. P., C. K. Folland, K. Maskell, J. A. Owen, and M. N. Ward (1992), Modelling the influence of global sea surface temperatures on the variability and predictability of seasonal Sahel rainfall, *Geophys. Res. Lett.*, *19*, 905–908, doi:10.1029/92GL00939.
- Waliser, D. E., and C. Gautier (1993), A satellite-derived climatology of the ITCZ, *J. Clim.*, *6*, 2162–2174, doi:10.1175/1520-0442(1993)006<2162:ASDCOT>2.0.CO;2.
- Wentz, F. J., C. L. Gentemann, D. K. Smith, and D. B. Chelton (2000), Satellite measurements of sea-surface temperature through clouds, *Science*, *288*, 847–850, doi:10.1126/science.288.5467.847.
- Wong, S., A. E. Dessler, N. H. Mahowald, P. Yang, and Q. Feng (2009), Maintenance of the lower tropospheric temperature inversion in the Saharan air layer by dust and dry anomaly, *J. Clim.*, *22*, 5149–5162, doi:10.1175/2009JCLI2847.1.
- Zhu, A., V. Ramanathan, F. Li, and D. Kim (2007), Dust plumes over the Pacific, Indian, and Atlantic oceans: Climatology and radiative impact, *J. Geophys. Res.*, *112*, D16208, doi:10.1029/2007JD008427.

K.-M. Kim, K. M. Lau, and E. M. Wilcox, Laboratory for Atmospheres, NASA Goddard Space Flight Center, Code 613.2, Greenbelt, MD 20771, USA. (eric.m.wilcox@nasa.gov)